ARTICLE

Synthesis of Zn(II) coordination complexes, their molecular design and docking with SARS-CoV-2 RBD protein and Omicron spike protein

Simranjeet Singh[a], Mukesh Choudhary[a]*

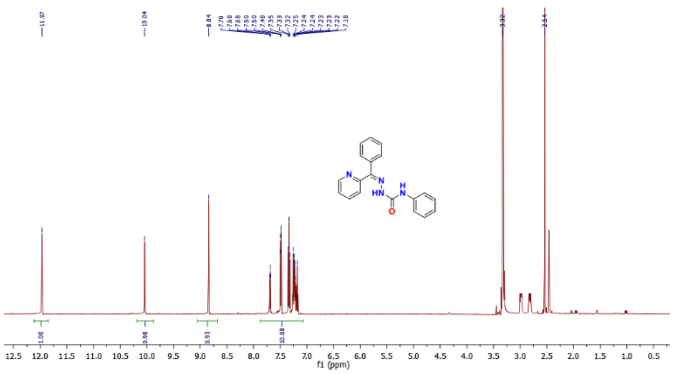

Figure S1. ^{1}H-NMR spectra of Schiff base ligand (L) in DMSO-d6 solution.

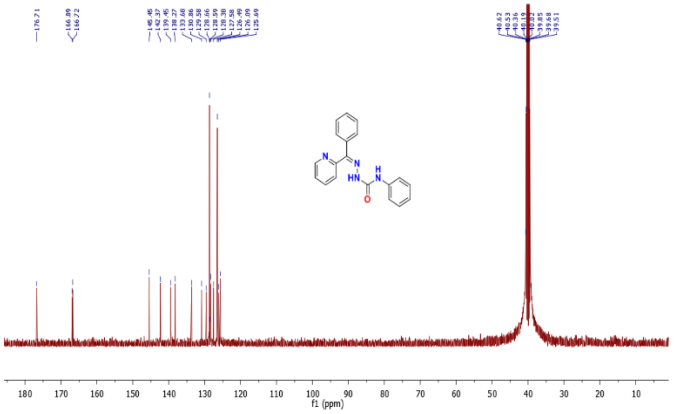

Figure S2. ^{13}C-NMR spectra of Schiff base ligand (L) in DMSO-d6 solution.

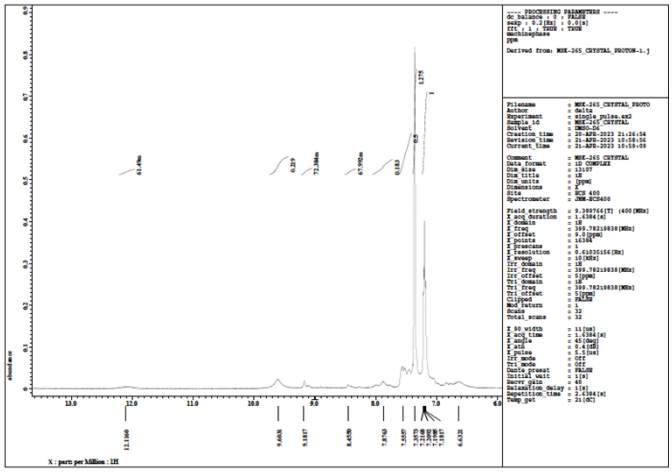

Figure S3. ^{1}H-NMR spectra of the zinc(II) complex [Zn(L)(en)]ClO_4(**1**) in DMSO-d6 solution.

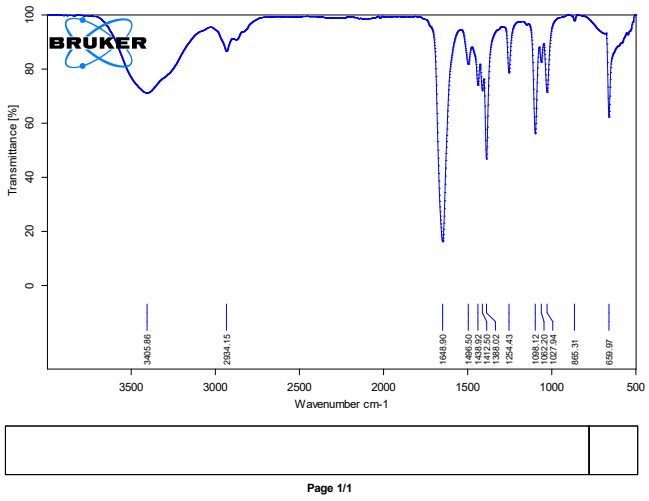

[a] *Department of Chemistry, National Institute of Technology Patna, Patna-800005 (Bihar) India.*

[a.] *Corresponding author: mukesh@nitp.ac.in*

Figure S4. FT-IR spectra of zinc(II) complex [Zn(L)(en)]ClO_4(**1**).

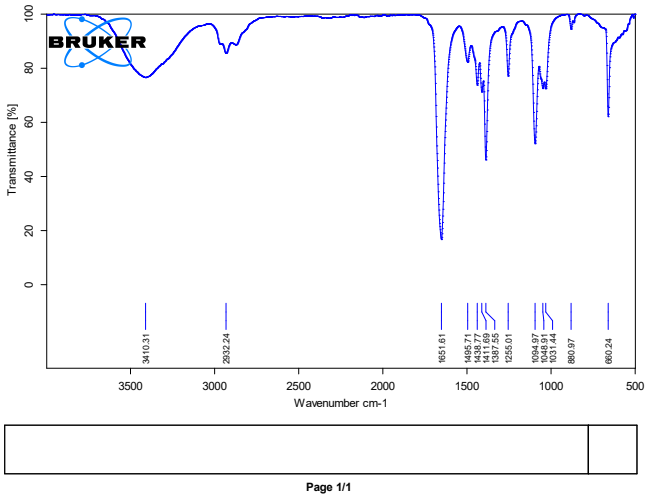

Figure S5. FT-IR spectra of zinc(II) complex [$Zn(L)_2$] (**2**).

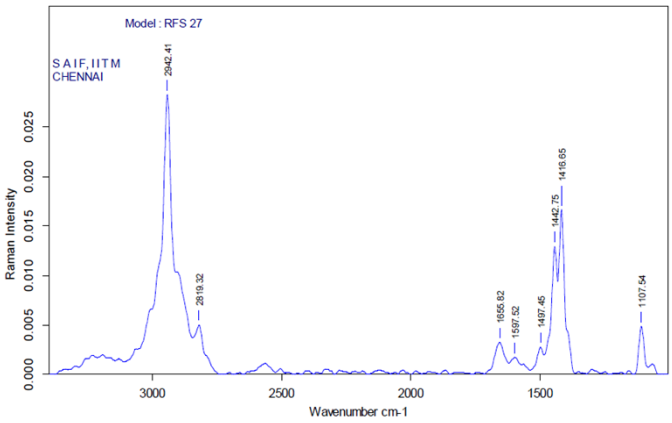

Figure S6. FT-Raman spectra of zinc (II) complex [Zn(L)(en)]ClO_4(**1**).

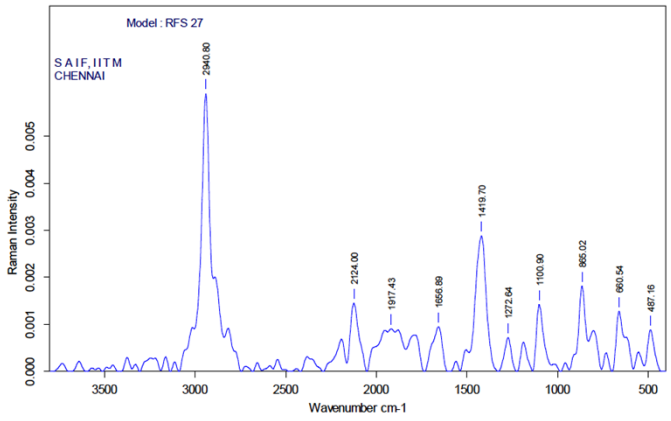

Figure S7. FT-Raman spectra of zinc(II) complex [$Zn(L)_2$] (**2**).

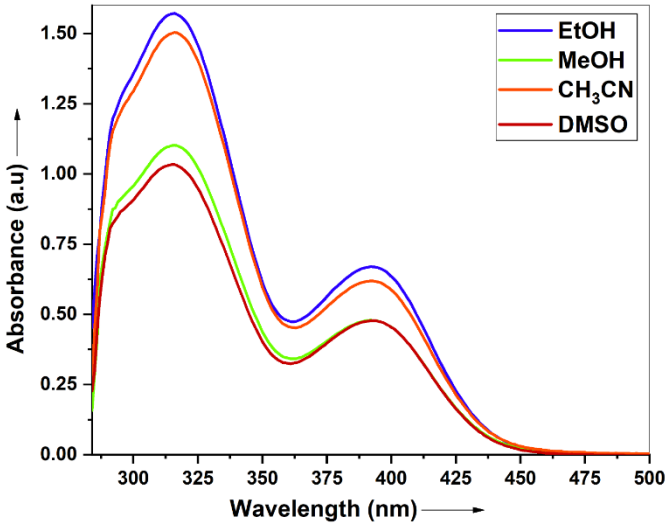

Figure S8. UV-Vis spectrum of Zn(II) complex [Zn(L)(en)]ClO_4 (**1**) in different solvents (3 x 10^{-3} M) at room temperature.

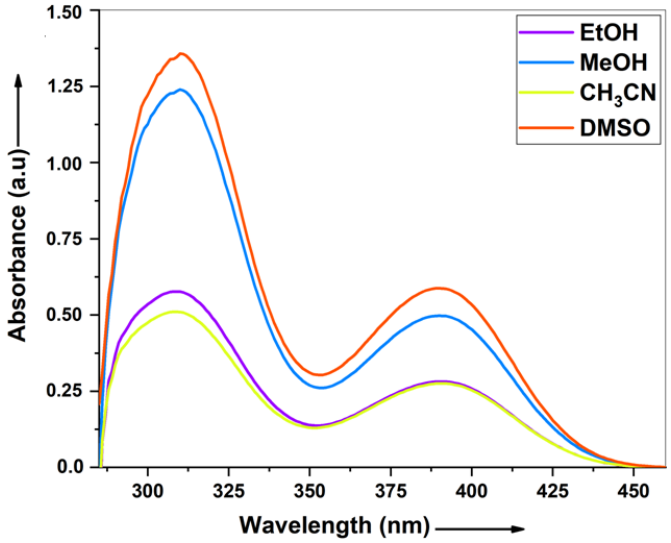

Figure S9. UV-Vis spectrum of Zn(II) complex [$Zn(L)_2$] (**2**) in different solvents (3 x 10^{-3} M) at room temperature.

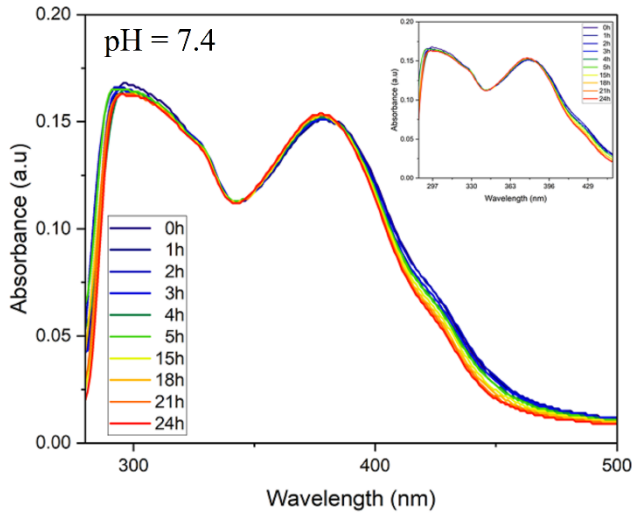

Figure S10. Time dependent absorption spectra of Zn(II) complex [Zn(L)(en)]ClO_4(**1**) in buffer solution at pH =7.4; Inset: the expanded region depicting the stability of the complex in buffer medium.

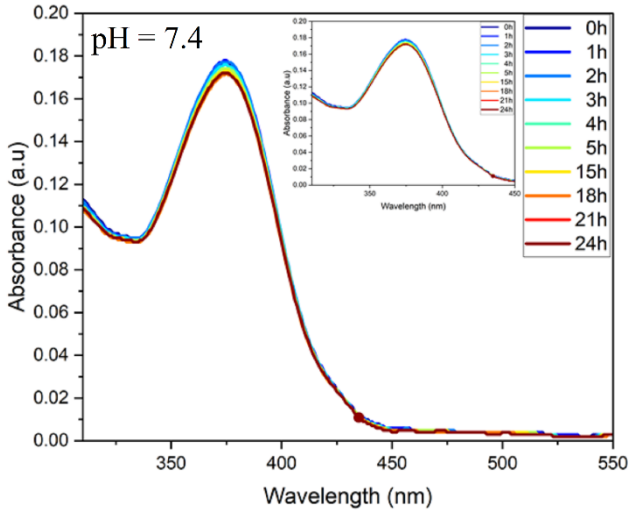

Figure S11. Time dependent absorption spectra of Zn(II) complex [$Zn(L)_2$](**2**) in buffer solution at pH =7.4; Inset: the expanded region depicting the stability of the complex in buffer medium.

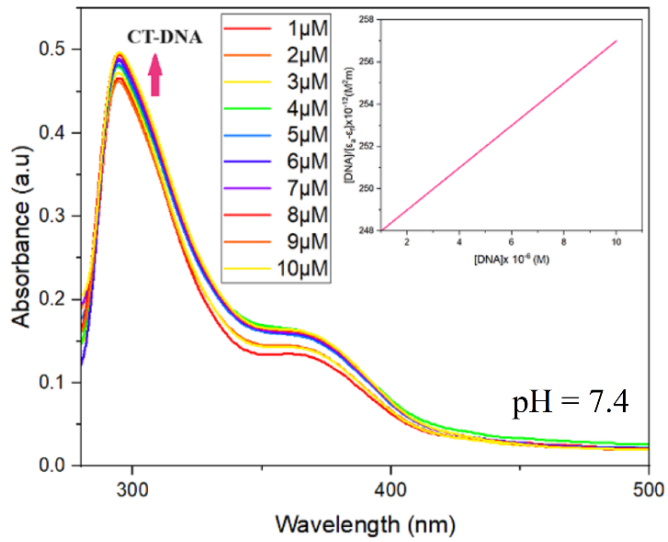

Figure S12. Absorption titration spectra upon incremental addition of CT-DNA to Zn(II) complex [Zn(L)(en)]ClO_4(**1**) solution. [Inset: the linear fitting to determine binding constant (K_b= 4.75 x 10^4 L mol^{-1}).

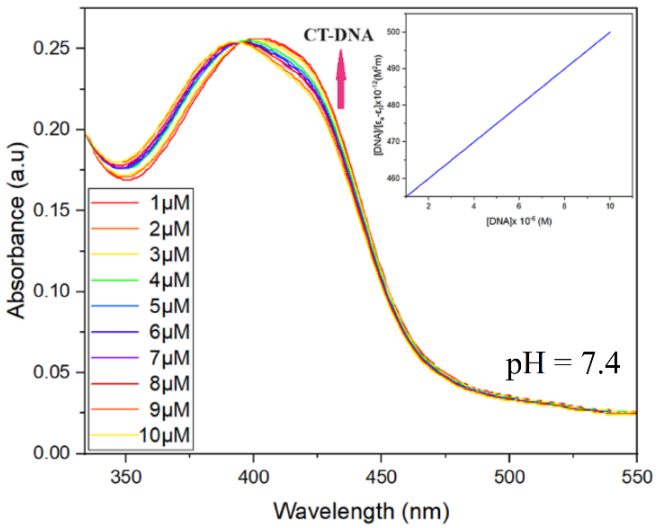

Figure S13. Absorption titration spectra upon incremental addition of CT-DNA to Zn(II) complex [$Zn(L)_2$](**2**) solution. [Inset: the linear fitting to determine binding constant (K_b= 5.82 x 10^4 L mol^{-1}).

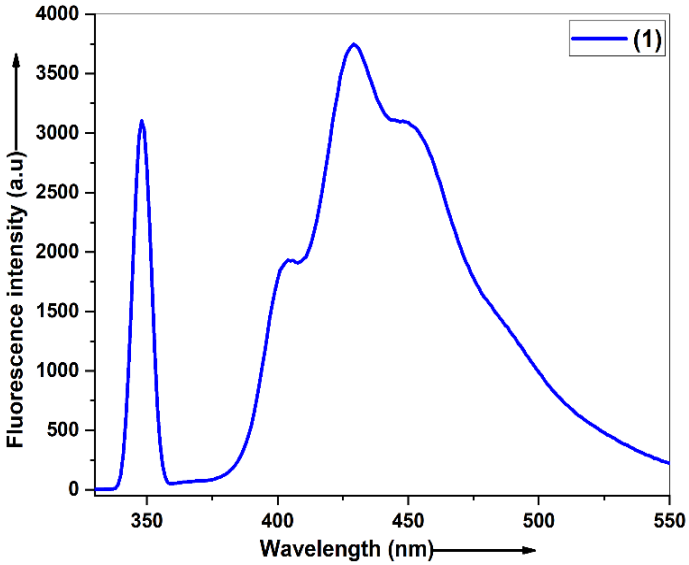

Figure S14. Fluorescence spectra of the Zn(II) complex [Zn(L)(en)]ClO_4(**1**) in MeOH (3x10^{-3} M) at room temperature.

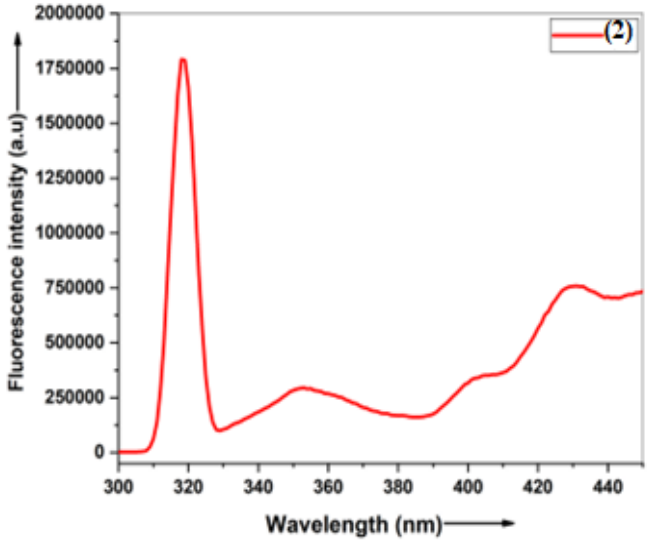

Figure S15. Fluorescence spectra of Zn(II) complex $[Zn(L)_2]$(**2**) in MeOH ($3x10^{-3}$ M) at room temperature.

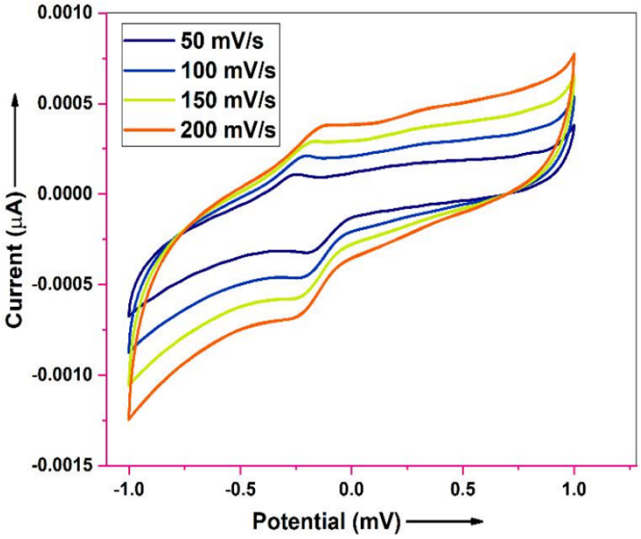

Figure S16. Cyclic voltammogram of the Zn(II) complex $[Zn(L)(en)]ClO_4$(**1**) with scan rate 50-200mV/sec in DMSO with TBAP (1mM) as supporting electrolyte.

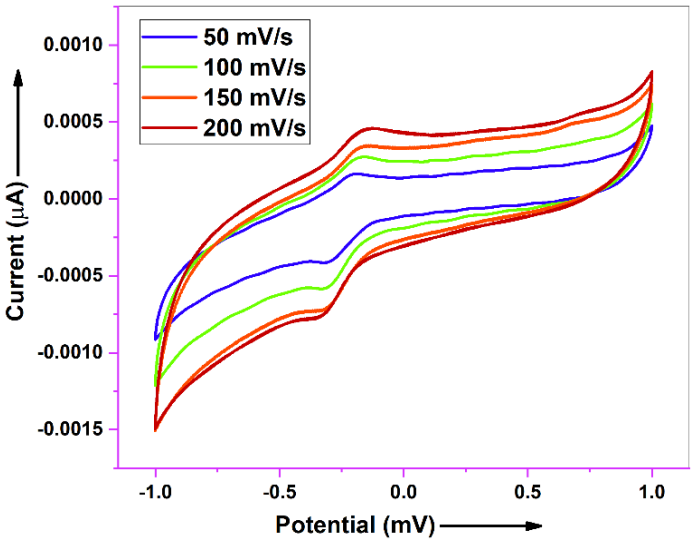

Figure S17. Cyclic voltammogram curve of the Zn(II) complex $[Zn(L)_2]$(**2**) with scan rate 50-200mV/sec in DMSO with TBAP (1mM) as supporting electrolyte.

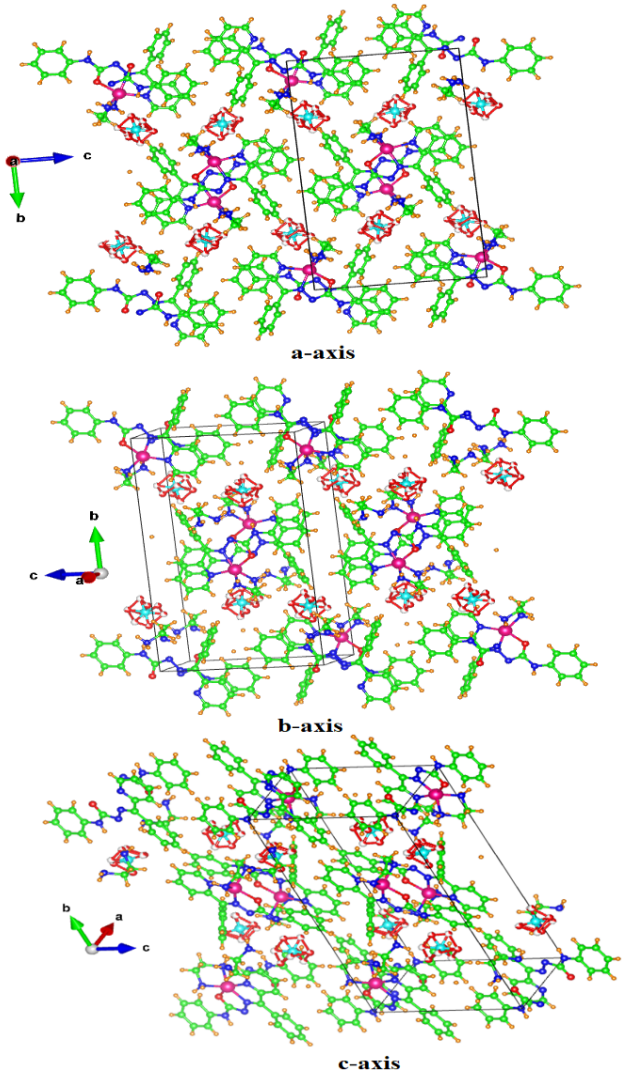

Figure S18. The packing view of the Zn(II) complex Zn(L)(en)]ClO_4 (**1**)(along *a-c axis*).

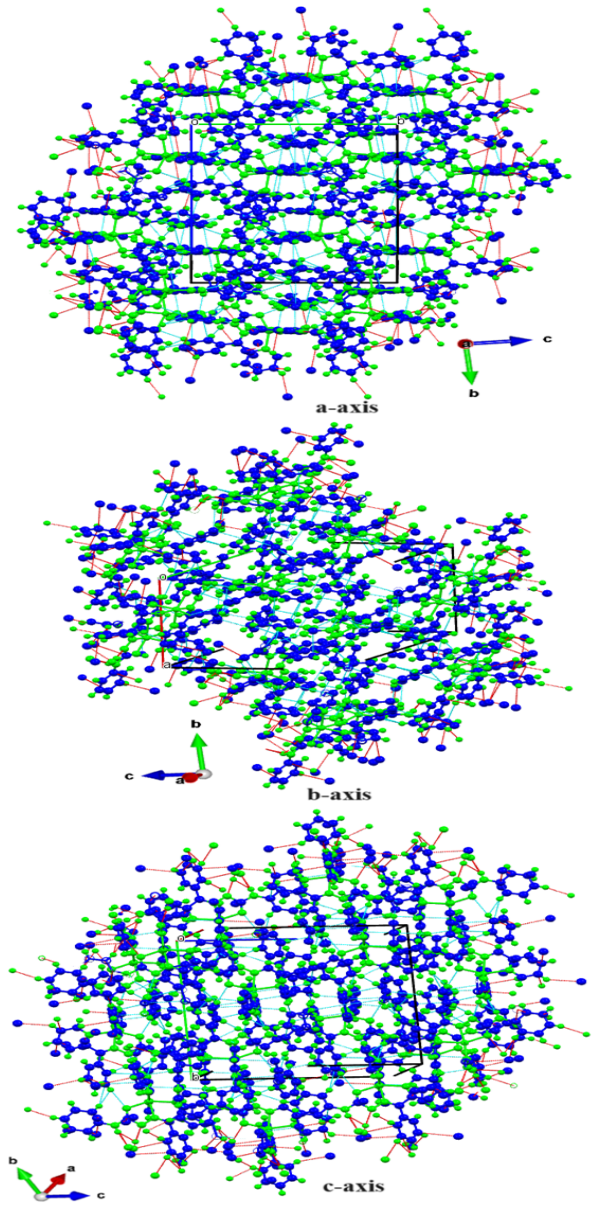

Figure S19. The packing view of the Zn(II) complex $[Zn(L)_2]$ (**2**)(along *a-c axis*).

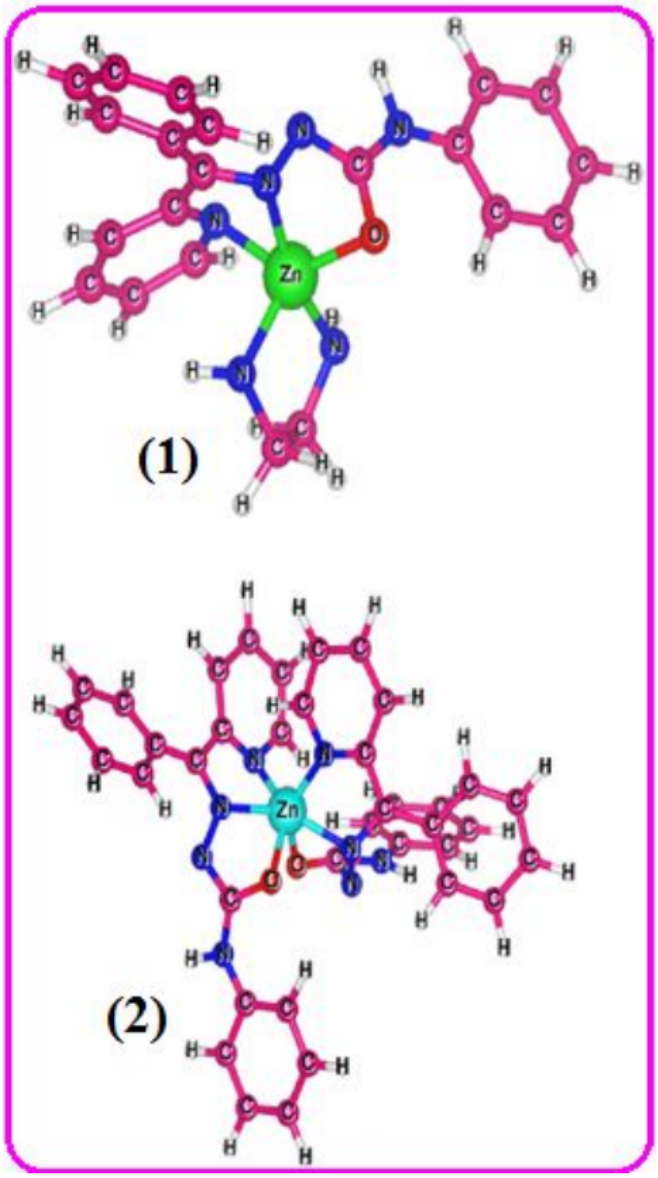

Figure S20. Optimized geometry of the newly synthesized Zn(II) complexes [Zn(L)(en)]ClO_4(**1**) and $[Zn(L)_2]$ (**2**).

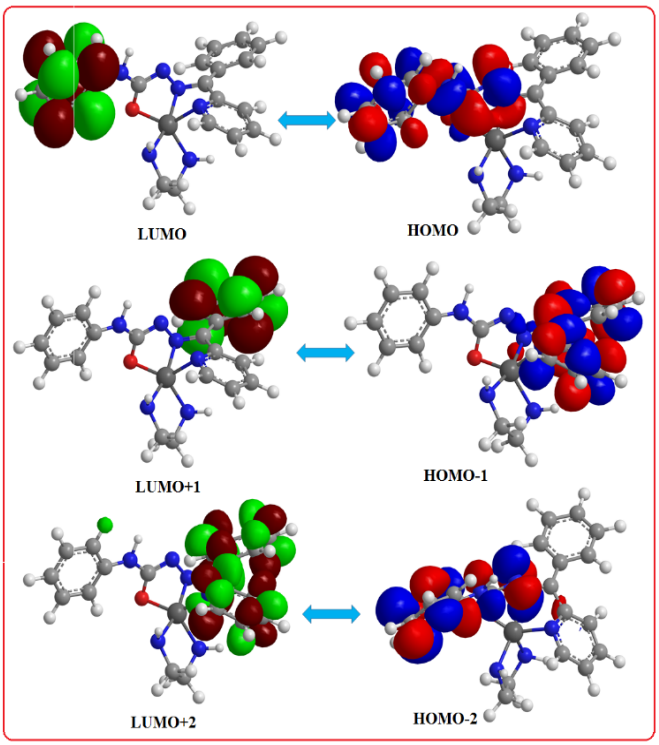

Figure S21. The atomic orbital composition of the frontier molecular orbitals (FMOs) plots of the cationic Zn(II) complex $[Zn(L)(en)]^+$(**1**).

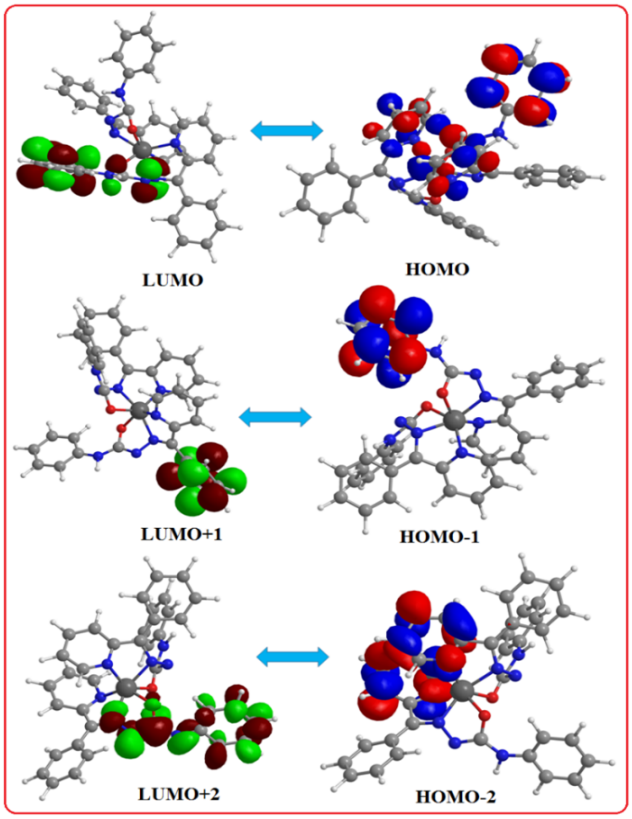

Figure S22. The atomic orbital composition of the frontier molecular orbitals (FMOs) plots of the Zn(II) complex $[Zn(L)_2]$(**2**).

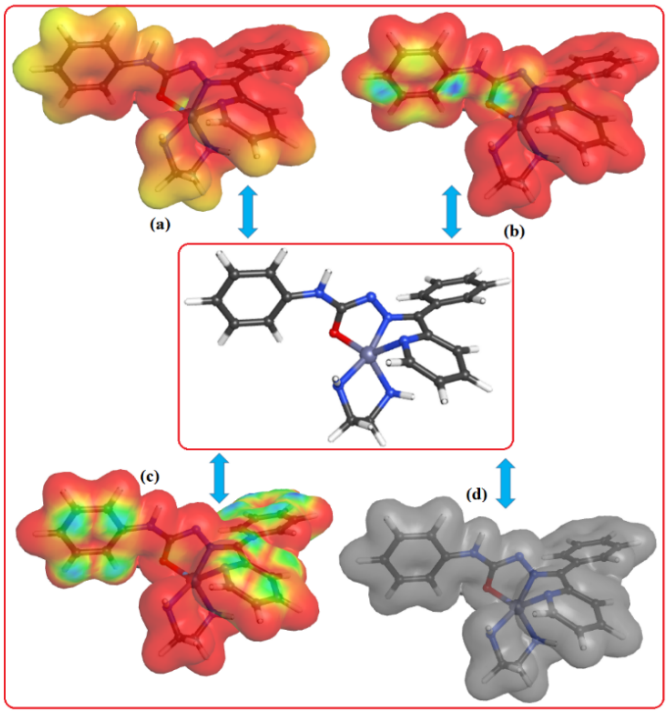

Figure S23. 3D-Molecular electrostatic potential (MEPs) plots of the cationic Zn(II) complex $[Zn(L)(en)]^+$(**1**).

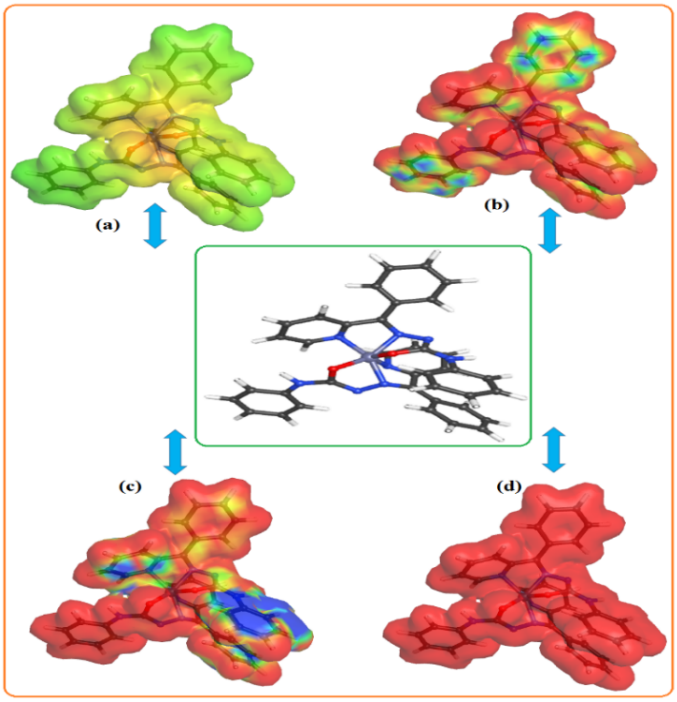

Figure S24. 3D-Molecular electrostatic potential (MEPs) plots of the Zn(II) complex $[Zn(L)_2]$(**2**).

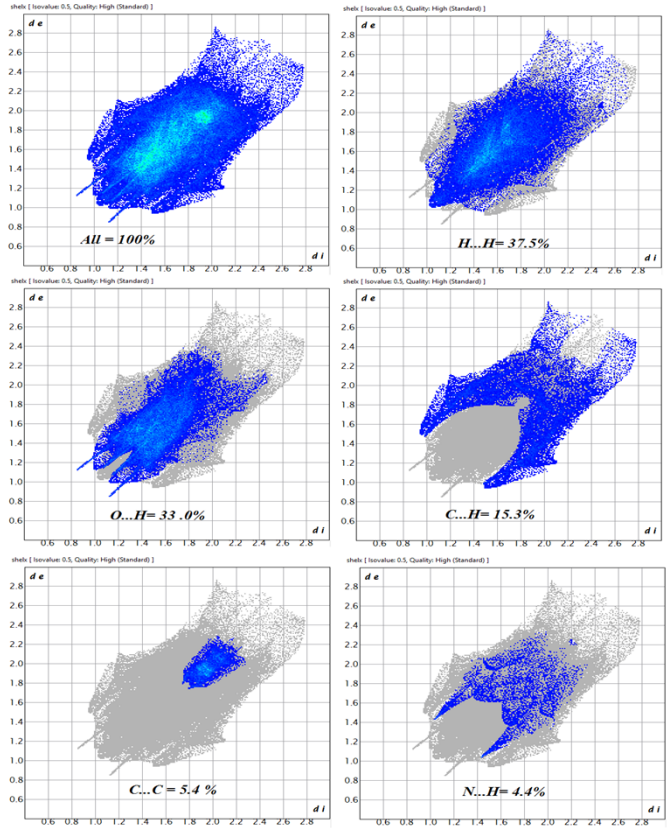

Figure S25. Graphical view with 2D Fingerprint plots for the Zn(II) complex [Zn(L)(en)]ClO_4(**1**) that showing percentage of contacts contributed to the total Hirshfeld surface (HS) area of the molecules; d_i and d_e are the distances from the surface to the nearest atoms interior and exterior to the surface respectively.

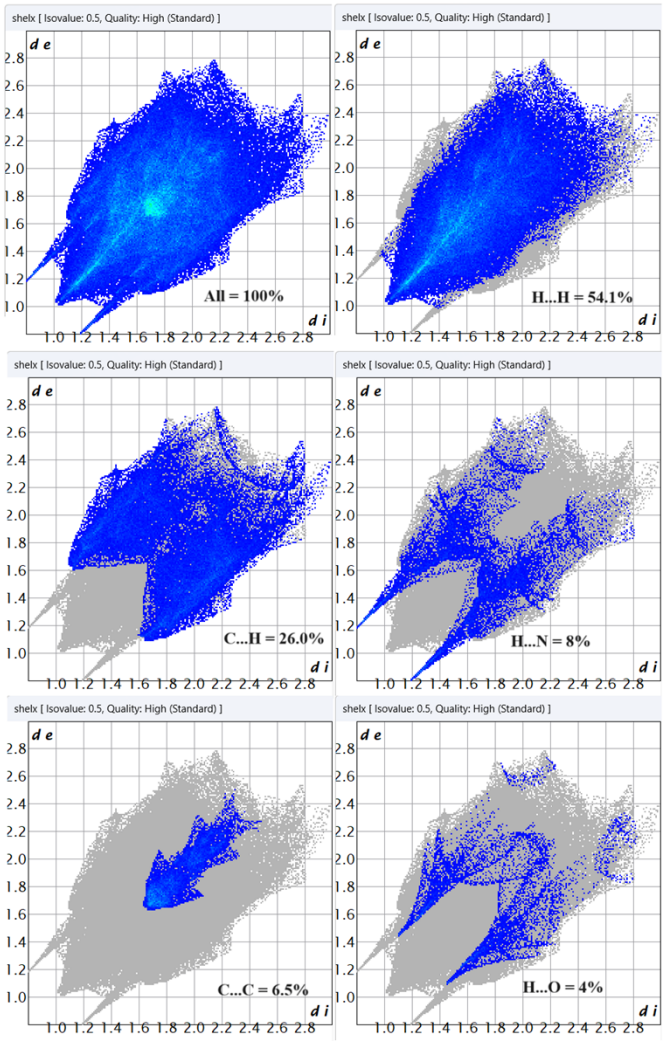

Figure S26. Graphical view with 2D Fingerprint plots for the Zn(II) complex [$Zn(L)_2$](**2**) that showing percentage of contacts contributed to the total Hirshfeld surface (HS) area of the molecules; d_i and d_e are the distances from the surface to the nearest atoms interior and exterior to the surface respectively.

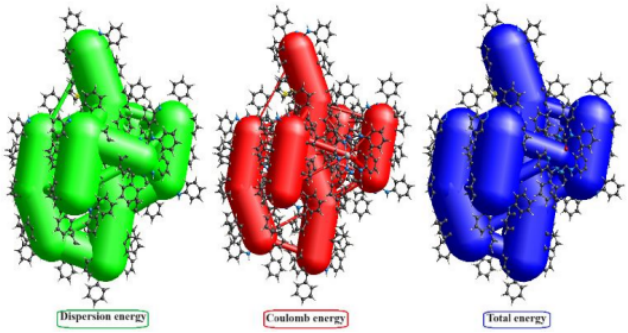

Figure S27. 3D graphical view of energy framework diagram for the Zn(II) complex $[Zn(L)_2]$(**2**); (a) Dispersion energy (E_{dis}), (b) Coulomb energy (E_{coul}), (c) Total energy (E_{tot}). Hydrogen atoms is omitted for clarity and all diagrams used the same cylindrical scale of 300 for energies.

Interaction Energies (kJ/mol)
R is the distance between molecular centroids (mean atomic position) in Å.

Total energies, only reported for two benchmarked energy models, are the sum of the four energy components, scaled appropriately (see the scale factor table below)

	N	Symop	R	Electron Density	E_ele	E_pol	E_dis	E_rep	E_tot
	1	-x, -y, -z	4.18	HF/3-21G	-21.4	-38.8	-130.9	48.3	-125.8
	1	x+1/2, -y+1/2, z+1/2	13.20	HF/3-21G	0.0	-1.5	0.0	0.0	-1.0
	1	-x, -y, -z	15.07	HF/3-21G	0.0	-0.6	0.0	0.0	-0.4
	1	x+1/2, -y+1/2, z+1/2	12.82	HF/3-21G	0.0	-1.6	0.0	0.0	-1.0
	1	-	6.58	HF/3-21G	0.0	nan	0.0	0.0	nan
	1	-	8.76	HF/3-21G	-9.3	0.0	-37.5	13.1	-32.6
	1	x, y, z	7.65	HF/3-21G	20.9	-2.3	-6.6	0.0	13.8
	1	-	11.26	HF/3-21G	0.0	-0.2	0.0	0.0	-0.1
	0	-x, -y, -z	13.67	HF/3-21G	0.0	-0.4	0.0	0.0	-0.3
	1	x, y, z	13.46	HF/3-21G	0.0	-1.7	0.0	0.0	-1.1
	1	-x+1/2, y+1/2, -z+1/2	12.94	HF/3-21G	0.0	-1.5	0.0	0.0	-1.0
	1	-	9.20	HF/3-21G	0.0	-1.5	0.0	0.0	-1.0
	1	-x, -y, -z	3.84	HF/3-21G	-75.4	-47.5	-132.1	53.3	-183.5
	1	-x+1/2, y+1/2, -z+1/2	13.65	HF/3-21G	0.0	-1.7	0.0	0.0	-1.1
	0	-	6.41	HF/3-21G	20.9	-2.3	-6.6	0.0	13.8
	1	-	6.35	HF/3-21G	-21.4	-38.8	-130.9	48.3	-125.8
	0	-	9.27	HF/3-21G	0.0	-1.5	0.0	0.0	-1.0
	1	-	7.94	HF/3-21G	0.0	-1.6	0.0	0.0	-1.0
	0	-	10.79	HF/3-21G	0.0	-1.7	0.0	0.0	-1.1

Scale factors for benchmarked energy models
See Mackenzie et al. IUCrJ (2017)

Energy Model	k_ele	k_pol	k_disp	k_rep
CE-HF ... HF/3-21G electron densities	1.019	0.651	0.901	0.811
CE-B3LYP ... B3LYP/6-31G(d,p) electron densities	1.057	0.740	0.871	0.618

Figure S28. Energy framework CE-B3LYP estimates of energy components and total energies (kJ/mol) for the closest intermolecular interactions in the Zn(II) complex $[Zn(L)(en)]ClO_4$(**1**).

Interaction Energies (kJ/mol)
R is the distance between molecular centroids (mean atomic position) in Å.

Total energies, only reported for two benchmarked energy models, are the sum of the four energy components, scaled appropriately (see the scale factor table below)

	N	Symop	R	Electron Density	E_ele	E_pol	E_dis	E_rep	E_tot
	1	x+1/2, -y+1/2, z+1/2	10.67	B3LYP/6-31G(d,p)	-10.4	-3.6	-58.4	37.3	-41.5
	0	-x, -y, -z	15.64	B3LYP/6-31G(d,p)	-4.1	-0.4	-11.8	0.0	-14.8
	0	-x, -y, -z	11.93	B3LYP/6-31G(d,p)	-0.5	-0.3	-19.2	8.1	-12.5
	1	x+1/2, -y+1/2, z+1/2	12.01	B3LYP/6-31G(d,p)	-8.9	-1.9	-29.9	0.0	-36.9
	0	-x, -y, -z	9.84	B3LYP/6-31G(d,p)	-8.4	-2.0	-89.9	44.4	-61.2
	1	x, y, z	11.17	B3LYP/6-31G(d,p)	-4.1	-1.8	-29.2	14.8	-22.0
	1	-x+1/2, y+1/2, -z+1/2	8.77	B3LYP/6-31G(d,p)	-59.4	-18.1	-120.1	97.4	-120.6
	0	x, y, z	16.93	B3LYP/6-31G(d,p)	0.6	-0.1	-4.6	0.0	-3.4
	0	-x, -y, -z	14.06	B3LYP/6-31G(d,p)	-1.4	-0.6	-12.8	0.0	-13.1

Scale factors for benchmarked energy models
See Mackenzie et al. IUCrJ (2017)

Energy Model	k_ele	k_pol	k_disp	k_rep
CE-HF ... HF/3-21G electron densities	1.019	0.651	0.901	0.811
CE-B3LYP ... B3LYP/6-31G(d,p) electron densities	1.057	0.740	0.871	0.618

Figure S29. Energy framework CE-B3LYP estimates of energy components and total energies (kJ/mol) for the closest intermolecular interactions in the Zn(II) complex $[Zn(L)_2]$ (**2**).

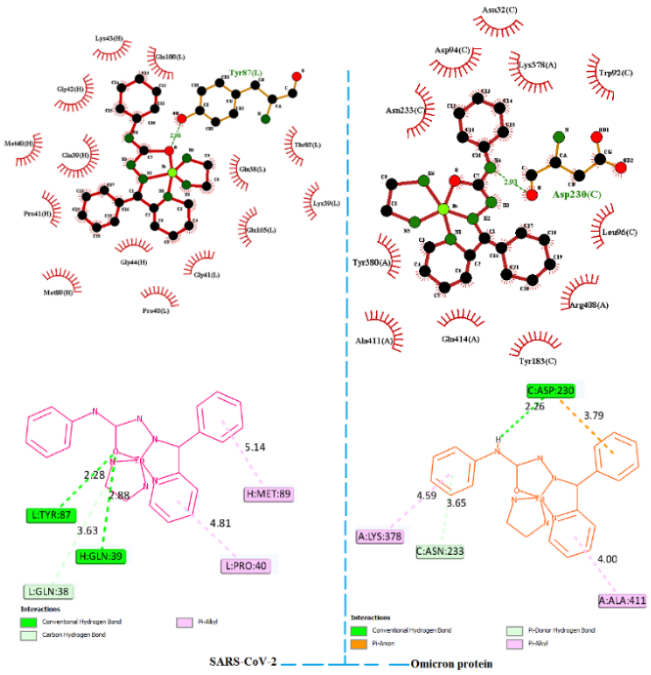

Figure S30. The top figures (Left-Right) show 3D view of the docked Zn(II) complex$[Zn(L)(en)]ClO_4$(**1**) with interacting residues inside the active site of the SARS-CoV-2 spike protein(PDB ID: 7LM9) and Omicron S protein PDB ID: 7WOP). The bottom figures (Left-Right) show the 2D representation with types of interactions.

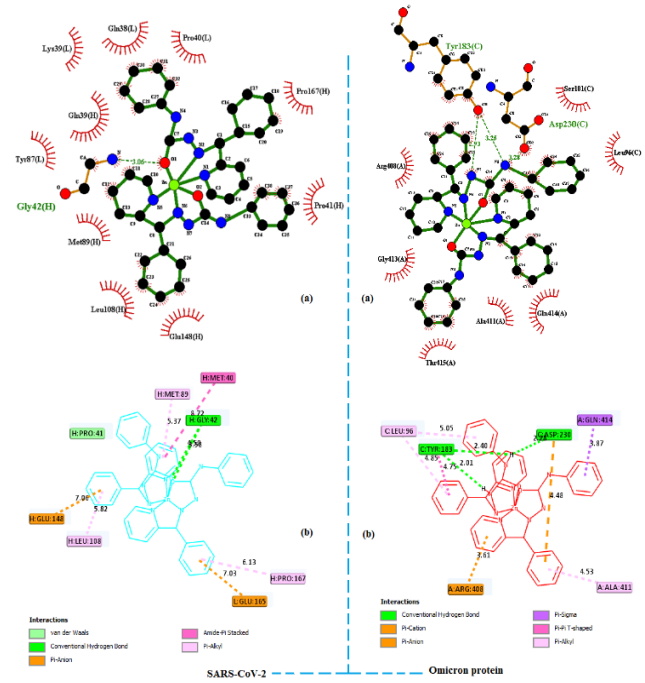

Figure S31. The top figures (Left-Right) show 3D view of the docked Zn(II) complex $[Zn(L)_2]$ (**2**) with interacting residues inside the active site of the SARS-CoV-2 receptor binding domain protein(PDB ID: 7LM9) and Omicron S protein (PDB ID: 7WOP). The bottom figures (Left-Right) show the 2D representation with types of interactions.

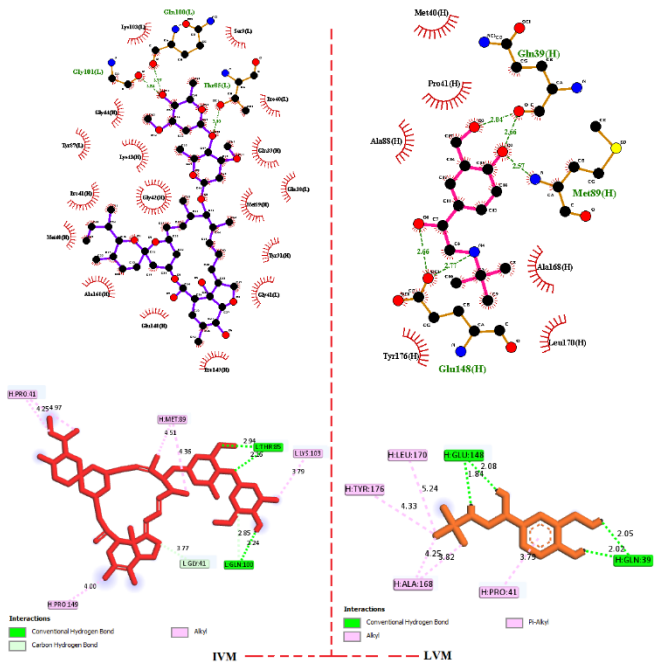

Figure S32. The top figures (Left-Right) show 3D view of ivermectin (IVM) and levosalbutamol (LVM) with interacting residues inside SARS-CoV-2 spike protein receptor-binding domain (PDB ID: 7LM9). The bottom figures (Left-Right) show the 2D representation of docked ivermectin (IVM) and levosalbutamol (LVM) with types of interactions.

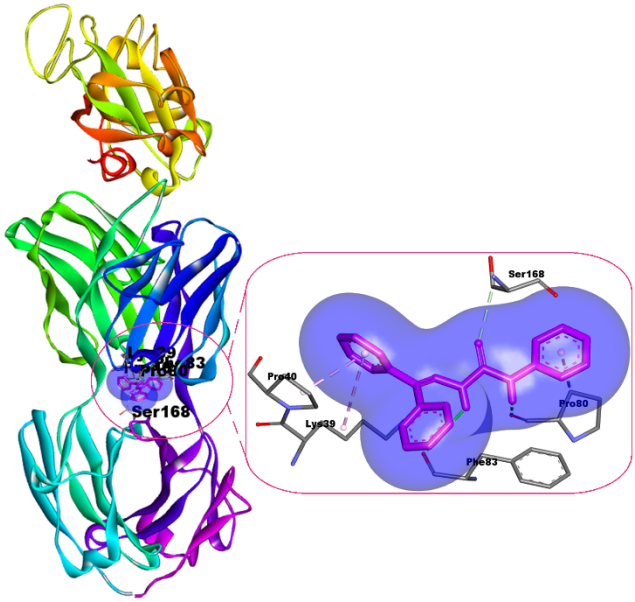

Figure S33. Graphical view of the docked Schiff base ligand (L) inside the active site of the SARS-CoV-2 RBD protein (PDB ID: 7LM9) with its focused view for interacting amino acid residues.

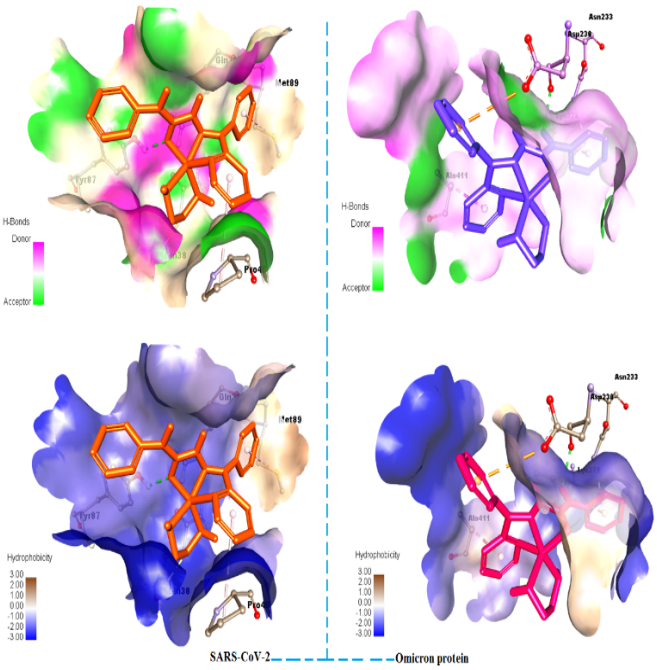

Figure S34. The top figures (Left-Right) show H-bond and Hydrophobicity representation of the docked Zn(II) complex $[Zn(L)(en)]ClO_4$(**1**) with interacting residues inside the active site of the SARS-CoV-2 RBD protein(PDB ID: 7LM9) and Omicron spike protein PDB ID: 7WOP). The bottom figures (Left-Right) show the 2D representation with types of interactions.

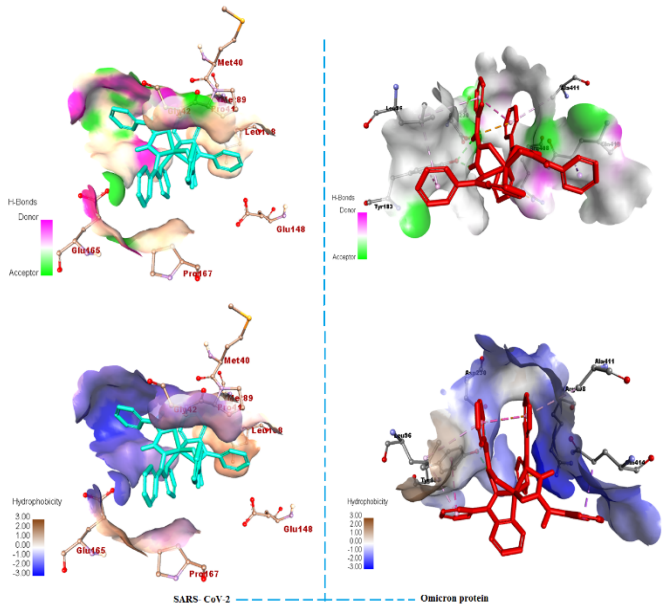

Figure S35. The top figures (Left-Right) show H-bond interactions of the docked Zn(II) complex $[Zn(L)_2]$(**2**) with interacting residues inside receptor-binding domain protein of the SARS-CoV-2 and Omicron S protein. The bottom figures (Left-Right) show the Hydrophobicity representation of the docked Zn(II) complex $[Zn(L)_2]$(**2**) with interacting residues inside receptor-binding domain protein of the SARS-CoV-2 and Omicron S protein.

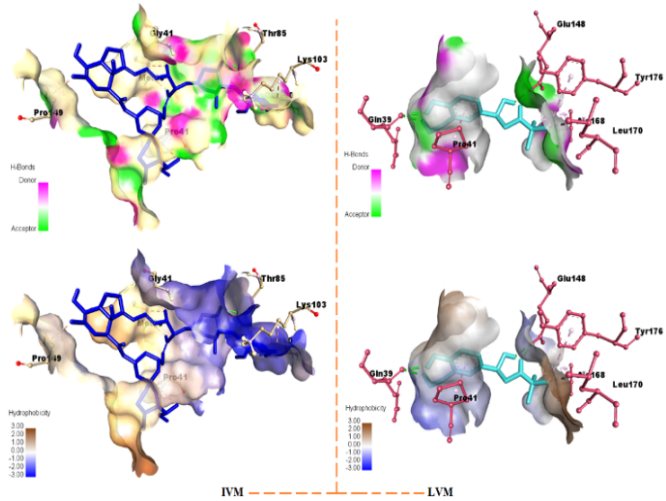

Figure S36. The top figures (Left-Right) show H-bond representation of ivermectin (IVM) and levosalbutamol (LVM) with interacting residues inside SARS-CoV2 RBD protein (PDB ID: 7LM9). The bottom figures (Left-Right) show the Hydrophobicity representation of docked ivermectin (IVM) and levosalbutamol (LVM) with types of interactions; hydrophobic pocket represented with yellow and blue colours, respectively.

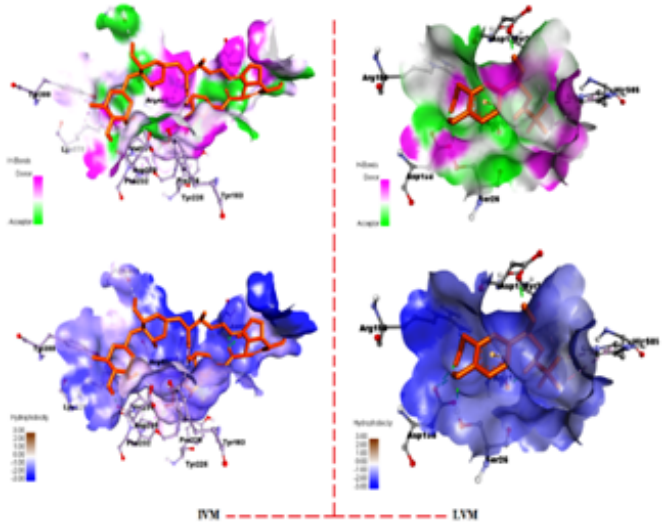

Figure S37. The top figures (Left-Right) show H-bond representation of ivermectin (IVM) and levosalbutamol (LVM) with interacting residues inside Omicron spike protein (PDB ID: 7WOP). The bottom figures (Left-Right) show the Hydrophobicity representation of docked ivermectin (IVM) and levosalbutamol (LVM) with types of interactions; hydrophobic pocket represented with orange and blue colours, respectively.

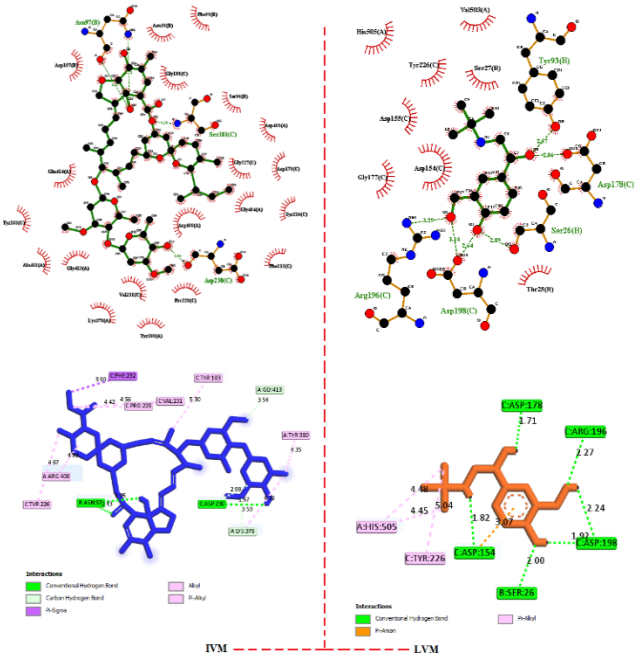

Figure S38. The top figures (Left-Right) show 3D view of ivermectin (IVM) and levosalbutamol (LVM) with interacting residues inside Omicron spike protein (PDB ID: 7WOP). The bottom figures (Left-Right) show the 2D representation of docked ivermectin (IVM) and levosalbutamol (LVM) with types of interactions.

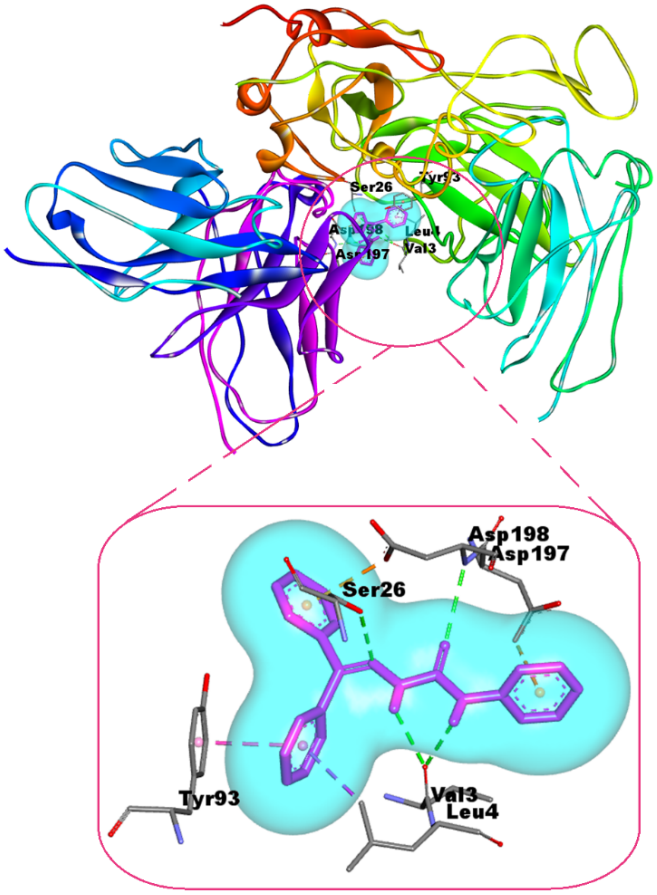

Figure S39. Graphical view of the docked Schiff base ligand (L) inside the active site of the SARS-CoV-2 Omicron spike protein (PDB ID: 7WOP) with its focused view for interacting amino acid residues.

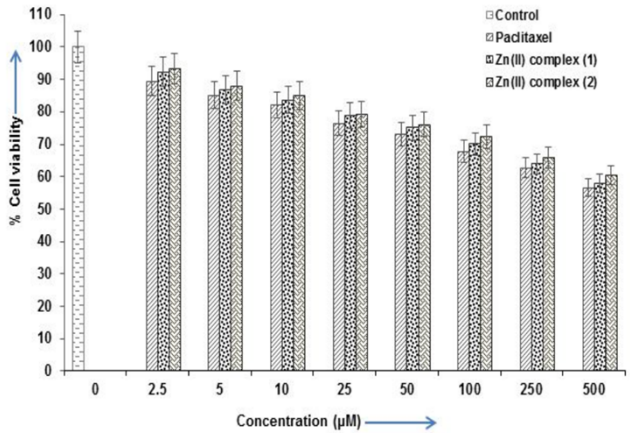

Figure S40. Percentage of Cell viability of HEK 293 cells with increasing concentration of the Zn(II) complex [Zn(L)(en)]ClO_4(**1**) and [$Zn(L)_2$] (**2**) (0–500 μM) as quantified by MTT assay.

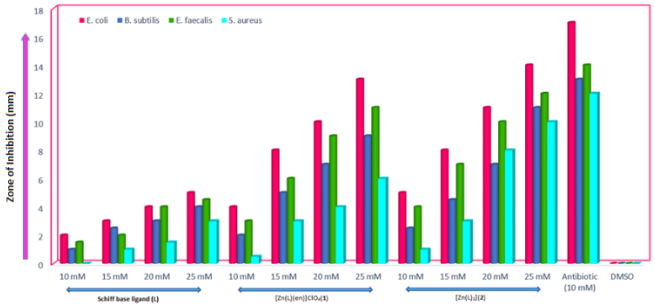

Figure S41. Graphical representation of anti-bacterial activity of the Zn(II) complexes [Zn(L)(en)]ClO_4(**1**) and [$Zn(L)_2$](**2**) as well as ligand (L) and standard antibiotic.

Table S1. The cyclic voltammetry data of the newly synthesized Zn(II) complexes [Zn(L)(en)]ClO_4(**1**), and [$Zn(L)_2$] (**2**) in DMSO solution containing 1M-TBAP as supporting electrolytes at different scan rates.

Scan rate (m V/s)	E_{pc} (mV)	I_{pc} (μA)	E_{pa} (mV)	I_{pa} (μA)	ΔE_p (mV)	E'_0 (mV)	I_{pa}/I_p (μA)
(**1**)							
50	-0.175	-1.031	-0.256	2.691	-0.081	-0.215	-2.612
100	-0.205	-1.146	-0.217	-7.423	-0.012	-0.211	-2.613
150	-0.226	-1.323	-0.182	1.238	0.044	-0.204	-0.935
200	-0.228	-1.260	-0.122	1.082	0.106	-0.175	-0.858
(**2**)							
50	-0.307	-1.801	-0.209	3.450	0.098	-0.258	-1.915
100	-0.303	-1.799	-0.179	-2.610	0.124	-0.241	1.450
150	-0.308	-1.511	-0.165	2.088	0.143	-0.236	-1.381
200	-0.325	-1.731	-0.156	2.318	0.169	-0.240	-1.339

$\Delta E_p = E_{pa} - E_{pc}$; $E'_0(mV) = (E_{pa} + E_{pc})/2$

Table S2. Hydrogen bond parameters found in the Zn(II) complex [Zn(L)(en)]ClO_4(**1**) and [$Zn(L)_2$] (**2**).

D-H...A	d(D-H)	d(H...A)	d(D...A)	<(DHA)
[Zn(L)(en)]ClO_4(**1**)				
C(2)-H(2)...O(2'^b)#1	0.95	2.37	3.230(15)	149.8
C(15)-H(15)...O(4'^b)#2	0.95	2.58	3.464(12)	155.5
C(19)-H(19)...O(1)	0.95	2.28	2.869(3)	119.7
N(4)-H(4N)...O(2^a)#2	0.851(17)	2.150(18)	2.998(3)	174(3)
N(6)-H(6A)...O(2^a)#3	0.876(8)	2.137(19)	3.007(4)	172(3)
N(6)-H(6A)...O(3^a)#3	0.876(18)	2.60(3)	3.339(16)	143(3)
N(6)-H(6A)...O(3'^b)#3	0.876(18)	2.65(3)	3.395(16)	144(3)
N(5)-H(5B)...O(2^a)	0.894(18)	2.58(3)	3.153(4)	123(3)
N(5)-H(5B)...O(2'^b)	0.894(18)	2.49(3)	3.215(5)	138(3)
N(5)-H(5B)...O(4'^b)	0.894(18)	2.26(2)	3.142(9)	171(3)
N(6)-H(6B)...N(3)#4	0.889(18)	2.59(2)	3.374(3)	148(3)
[$Zn(L)_2$] (**2**)				
C(3)-H(3)....O(1)	0.95	2.27	2.8909(17)	121.9
C(26)-H(26)...O(2)	0.95	2.29	2.9032(17)	121.5
N(5)-H(5N)...N(2)#1	0.87(2)	2.20(2)	3.0617(15)	170.9(18)
N(1)-H(1N)...N(6)#2	0.87(2)	2.14(2)	2.9963(15)	171.9(18)

Symmetry transformations used to generate equivalent atoms:

#1 x-1/2,-y+3/2,z-1/2 #2 -x+1,-y+1,-z+1 #3 x-1,y,z #4 -x,-y+1,-z+1 for

[Zn(L)(en)]ClO_4(**1**); and #1-x+1/2, y+1/2, -z+1/2#2-x+1/2, y-1/2, -z+1/2 for [$Zn(L)_2$] (**2**)

Table S3. The HOMO and LUMO energies and the energy gap (ΔE_g) of the synthesized Zn(II) complex [Zn(L)(en)]ClO_4(**1**) and [$Zn(L)_2$] (**2**).

FOMs energies and the energy gap (ΔE_g)[a]	[Zn(L)(en)]ClO_4(**1**)	[$Zn(L)_2$] (**2**)
E_{LUMO}	6.51	6.33
E_{HOMO}	3.35	2.91
ΔE_g	3.16	3.42
$E_{LUMO\ (+1)}$	7.14	7.02
$E_{HOMO\ (-1)}$	4.16	2.38
ΔE_g	2.98	4.64
$E_{LUMO\ (+2)}$	6.94	7.31
$E_{HOMO\ (-2)}$	4.21	2.19
ΔE_g	2.73	5.12

[a] Energy gap (ΔE) = E_{LUMO}-$E_{HOMO;}$ units in eV

Table S4. Global reactivity descriptors of the synthesized Zn(II) complexes [Zn(L)(en)]ClO_4(**1**) and [$Zn(L)_2$] (**2**).

Molecular descriptors	Mathematical description	[Zn(L)(en)]ClO_4(**1**)	[$Zn(L)_2$] (**2**)
Ionization potential (IP)	IP = - E_{HOMO}	-3.35	-2.91
electron affinity (EA)	EA = -E_{LUMO}	-6.51	-6.33
electro negativity (χ)	χ = (IP + EA)/2	-4.93	-4.62
chemical potential (μ)	η = (IP - EA)/2	1.58	1.71
global softness (σ)	μ = -(IP + EA)/2	4.93	4.62
global hardness (η)	σ = 1/2η	0.32	0.29
Electrophilicity index (ω)	ω = μ^2 / 2 η	7.69	6.24

Table S5. AUTODOCK parameters (docking coordinates, grid size and grid spacing) used for ivermectin (IVM) and levosalbutamol (LVM) docked with SARS CoV-2 Spike protein receptor-binding domain (PDB ID: 7LM9) and the Omicron spike protein (PDB ID: 7WOP).

Autodock parameters	SARS-CoV-2 Spike protein (PDB ID:7LM9)		Omicron Spike proteins (PDB ID: 7WOP)	
	IVM	LVM	IVM	LVM
Docking coordinates (x, y, z)	68.25 70.13 78.65	68.56 71.37 70.68	72.95 70.82 72.28	80.56 82.67 86.34
Grid Size (x, y, z)	79.23 82.45 80.54	71.39 82.69 86.34	85.37 83.32 81.72	88.38 90.62 87.10
Grid spacing	0.375 Å	0.375 Å	0.375 Å	0.375 Å

Table S6. The relevant parameters obtained from AUTODOCK outputs for ivermectin(IVM) and levosalbutamol (LVM) with SARS CoV-2 Spike protein receptor-binding domain (PDB ID: 7LM9) and the Omicron spike protein (PDB ID: 7WOP).

Property	SARS-CoV-2 Spike protein (PDB ID:7LM9)		Omicron Spike protein (PDB ID: 7WOP)	
	IVM	LVM	IVM	LVM
Binding energy (kcal/mol)	-9.98	-6.02	-7.68	-7.64
Ligand efficiency	-0.16	-0.35	-0.12	-0.45
Inhibition constant (μM or nM)	4.854 (4854)	3.891 (3891)	2.33 (2330)	2.51 (2510)
Intermolecular Energy (kcal/mol)	-13.26	-8.4	-10.96	-10.03
vdW + Hbond + desolv Energy (kcal/mol)	-13.14	-8.01	-10.55	-7.38
Electrostatic energy (kcal/mol)	-0.12	-0.39	-0.41	-2.65
Total internal Energy (kcal/mol)	-2.79	-1.12	-2.73	-1.47
Torsional energy (kcal/mol)	3.28	2.39	3.28	2.39
Unbound Energy (kcal/mol)	-2.79	-1.12	2.73	-1.47
refRMS	48.27	54.36	329.24	357.31

Table S7. Established structure activity relationship (SAR) between the experimental geometries of the Zn(II) complexes [Zn(L)(en)]ClO_4(**1**) and [$Zn(L)_2$](**2**) determined by the single crystal X-ray diffraction technique and the theoretical geometries observed upon interactions against SARS-CoV-2 RBD protein (PDB ID: 7LM9) and Omicron S protein (PDB ID: 7WOP).

Complexes	Experimental bond lengths (Å)		Docked complexes inside SARS-CoV-2 RBD protein and Omicron S protein with bond lengths (Å)			
			PDB ID: 7LM9		PDB ID: 7WOP	
(**1**)	Zn(1)-N(2)	2.044(2)	Zn(1)-N(2)	2.031(4)	Zn(1)-N(2)	2.063(1)
	Zn(1)-N(5)	2.048(2)	Zn(1)-N(5)	2.024(5)	Zn(1)-N(5)	2.021(4)
	Zn(1)-N(6)	2.047(2)	Zn(1)-N(6)	2.032(4)	Zn(1)-N(6)	2.041(4)
	Zn(1)-O(1)	2.1117(17)	Zn(1)-O(1)	2.2214(8)	Zn(1)-O(1)	2.1314(2)
	Zn(1)-N(1)	2.127(2)	Zn(1)-N(1)	2.147(2)	Zn(1)-N(1)	2.123(1)
	N(2)-N(3)	1.363(3)	N(2)-N(3)	1.312(3)	N(2)-N(3)	1.312(5)
(2)	Zn(1)-N(3)	2.0756(10)	Zn(1)-N(3)	2.0746(4)	Zn(1)-N(3)	2.0736(5)
	Zn(1)-N(7)	2.0772(10)	Zn(1)-N(7)	2.0512(6)	Zn(1)-N(7)	2.0672(1)
	Zn(1)-O(1)	2.1024(9)	Zn(1)-O(1)	2.1031(8)	Zn(1)-O(1)	2.1044(9)
	Zn(1)-O(2)	2.1290(9)	Zn(1)-O(2)	2.1260(9)	Zn(1)-O(2)	2.1250(9)
	Zn(1)-N(4)	2.1898(11)	Zn(1)-N(4)	2.1875(10)	Zn(1)-N(4)	2.1868(4)
	Zn(1)-N(8)	2.2163(11)	Zn(1)-N(8)	2.2143(1)	Zn(1)-N(8)	2.2263(10)
	N(2)-N(3)	1.3512(14)	N(2)-N(3)	1.3524(1)	N(2)-N(3)	1.3312(9)
	N(6)-N(7)	1.3488(14)	N(6)-N(7)	1.3442(8)	N(6)-N(7)	1.3468(5)

Table S8. Comparison of binding energies (ΔG) and inhibition / dissociation constants (K_i/K_d) of some metal complexes obtained from in-silico docking study.

Sl. No.	Complexes	binding energies (kcal/mol)	inhibition / dissociation constants, [Ki(μM)	References
1	$[Cu(L^1)_2]$	-8.7	2.585	42
2	$[Cu(L^2)(CH_3OH)(Cl)]$	-8.2	2.395	42
3	$[Cu(L^1)_2]$(**1**)	-9.8	2.912	41
4	$[Cu(L^2)_2]$(**2**)	-9.4	2.813	41
5	$[Ni(L^1)](PPh_3)]DMF$	-8.93	0.28461	43
6	$[Ni(L^2)]$	-5.7	65.87	43
7	$[Ni_3(\mu\text{-}L)_2(bipy)_3]$	-8.9	2.373	93
8	$[Ni(L^1)(Phen)_2]ClO_4$	-11.5	-	87(c)
9	$[Cu\ (L^2)]$	-8.5	-	87(c)
10	$[Ni(L)_2]$	-7.2	-	87(b)
11	$[Cu(L)_2]$	-9.7	-	87(b)
12	[Mo(dien)O3]	-9.9	6.539	94
13	[Zn(L)(en)]ClO_4(**1**)	-9.1 (-8.4)	2.938 (1.396)	This work
14	$[Zn(L)_2]$ (**2**)	-10.2 (-8.9)	1.296 (1.753)	This work

Table S9. Structure activity relationship (SAR) between the experimental geometries of the Zn(II) complexes [Zn(L)(en)]ClO_4(**1**) and [$Zn(L)_2$](**2**) determined by the single crystal X-ray diffraction technique and the theoretical geometries observed upon interactions with DNA binding protein (PDB ID: 7UV7).

Complexes	Experimental bond lengths (Å)		Docked complexes inside DNA binding protein with bond lengths (Å) (PDB ID: 7UV7)	
(**1**)	Zn(1)-N(2)	2.044(2)	Zn(1)-N(2)	2.024(2)
	Zn(1)-N(5)	2.048(2)	Zn(1)-N(5)	2.034(1)
	Zn(1)-N(6)	2.047(2)	Zn(1)-N(6)	2.022(3)
	Zn(1)-O(1)	2.1117(17)	Zn(1)-O(1)	2.24(5)
	Zn(1)-N(1)	2.127(2)	Zn(1)-N(1)	2.157(7)
	N(2)-N(3)	1.363(3)	N(2)-N(3)	1.332(1)
(2)	Zn(1)-N(3)	2.0756(10)	Zn(1)-N(3)	2.0326(1)
	Zn(1)-N(7)	2.0772(10)	Zn(1)-N(7)	2.0212(8)
	Zn(1)-O(1)	2.1024(9)	Zn(1)-O(1)	2.101(2)
	Zn(1)-O(2)	2.1290(9)	Zn(1)-O(2)	2.132(3)
	Zn(1)-N(4)	2.1898(11)	Zn(1)-N(4)	2.1235(3)
	Zn(1)-N(8)	2.2163(11)	Zn(1)-N(8)	2.2313(2)
	N(2)-N(3)	1.3512(14)	N(2)-N(3)	1.3144(2)
	N(6)-N(7)	1.3488(14)	N(6)-N(7)	1.3132(6)